

Article

Promoting Light Hydrocarbons Yield by Catalytic Hydrodechlorination of Residual Chloromethanes Using Palladium Supported on Zeolite Catalysts

Carlos Fernandez-Ruiz ¹, Jorge Bedia ^{1,*} , Javier Mario Grau ² , Ana Clara Romero ², Daniel Rodríguez ¹, Juan José Rodríguez ¹ and Luisa María Gómez-Sainero ¹ 

¹ Departamento de Ingeniería Química, Universidad Autónoma de Madrid, Cantoblanco, 28049 Madrid, Spain; carlos.fernandezruiz@uam.es (C.F.-R.); daniel.rodriguez@uam.es (D.R.); juanjo.rodriguez@uam.es (J.J.R.); luisa.gomez@uam.es (L.M.G.-S.)

² Instituto de Investigaciones en Catálisis y Petroquímica “Ing. José Miguel Parera”-INCAPE-(FIQ-UNL, CONICET), CCT CONICET Santa Fe “Dr. Alberto Cassano”, Colec. Ruta Nac. N° 168 KM 0 Paraje El Pozo, S3000AOJ Santa Fe, Argentina; jgrau@fiq.unl.edu.ar (J.M.G.); anaclararomero04@gmail.com (A.C.R.)

* Correspondence: jorge.bedia@uam.es; Tel.: +34-91-497-2911

Received: 14 January 2020; Accepted: 4 February 2020; Published: 6 February 2020



Abstract: Gas catalytic hydrodechlorination (HDC) of trichloromethane (TCM) and dichloromethane (DCM) was analyzed using Pd (1 wt.%) on different zeolites as catalysts. The aim of this study was to know the surface properties of the catalysts and reaction conditions that promote the yield to light hydrocarbons in this reaction. Five different zeolite supports were used from three commercial zeolites (KL, L-type; NaY, Faujasite; H-MOR, Mordenite). KL and NaY were submitted to ionic exchange treatments in order to increase their acidity and analyze the effect of the acidity in the activity and selectivity of the HDC reaction. Exchanged zeolites (HL and HY) showed the highest Pd dispersion due to their higher surface acidity. The best TCM/DCM conversion and selectivity to light hydrocarbons was obtained using the two non-exchanged zeolite-catalysts, KL and NaY. Low surface acidity seems to be the key aspect to promote the formation of light hydrocarbons. The formation of these products is favored at high reaction temperatures and low H₂: chloromethane ratios. KL showed the highest selectivity to olefins (60%), although with a lower dechlorination degree. Non-exchanged NaY catalyst showed high selectivity to paraffins (70% and 95% for the HDC of DCM and TCM, respectively).

Keywords: hydrodechlorination; trichloromethane; dichloromethane; paraffins; olefins; zeolites; palladium

1. Introduction

Chloromethanes are volatile organic compounds (VOCs) with one or more chlorine atoms. These compounds are released to the environment as a result of their use in different industrial applications [1]. Due to their hazardous characteristics for human health and environment, the difficult substitution in many industrial processes, and the increase in industrial emissions [2], governments are limiting their emissions through more stringent environmental regulations [3,4]. In this context, there is a growing interest in the research of the removal or degradation of chloromethanes from outlet gas streams. Most of the published works are focused mainly on the elimination of chloromethanes, with little attention to the selectivity of the reaction. However, the conversion of residual chloromethanes into high-value hydrocarbons, such as light olefins and paraffins, is a very interesting technological solution [5].

Light hydrocarbons, especially light olefins, have an important role in the petrochemical and pharmaceutical industries, as intermediates on the synthesis of many products. The main processes

to produce them are steam cracking, fluid-catalytic cracking, and catalytic hydrogenation, all of which are highly demanding on energy and capital [6]. In this context, there is much interest in the research and development of cheaper synthesis strategies. Catalytic hydrodechlorination (HDC) can be one of the alternatives considered to transform chlorinated compounds into more valuable light hydrocarbons. HDC has been extensively studied for the removal of chloromethanes due to the mild required conditions of pressure and temperature [7]. However, only a few works have reported high selectivity to olefins in the HDC reaction, using different types of supports and metallic active phases [8–12]. In most of those studies, deactivation and low concentration of chloromethane reactant considerably limited the possible application of the results. HDC catalysts frequently use noble metals as active phases because of their well-known high activity. The most commonly used are Pt, Pd, Rh, and Ru, on activated carbons, modified silica, zeolites, alumina, and recently carbon nanofibers and nanotubes [13–17].

Zeolites as supports have the advantage of tunable properties, such as acidity, textural porosity, well-defined structure, and in some cases, high specific surface area. Furthermore, as catalytic HDC is a sensitive structure reaction, the interest in using zeolite as support increases because of their capacity to encapsulate metal nanoparticles (NPs), protecting them against aggregation and sintering, which are very common phenomena when using noble metals active phases [18,19]. As the NPs are isolated from others NPs due to their encapsulation on the zeolite cages and different channels, the catalytic activity can be improved, as well as the stability [20]. Due to this, zeolites are commonly used in liquid phase hydrodechlorination reactions [13,21,22], however, fewer studies have been applied to gas phase HDC [23–26]. In those gas-phase studies, conversion usually decreased after a few hours on stream, high selectivities to methane were obtained, and/or very low reactant inlet concentrations (below 100 ppm) were used [23,27,28]. Hereunder, we summarize some of the results reported about gas-phase HDC of different chlorine compounds (not necessarily chloromethanes) on zeolite catalysts, which can be found in the literature. Srebowata et al. reported high selectivity to ethylene (75%) in the HDC of 1,2-dichloroethane using bimetallic Ag-Cu particles supported on β -zeolites [23] and Ni on BEA-zeolites [24]. Nevertheless, the stability of the catalysts was poor, and the conversion decreased down to 6% after a few hours on stream, despite chloroethane molecules being usually more reactive than chloromethanes in HDC reaction. Pd and Pt supported on zeolites were used as catalysts in the HDC of carbon tetrachloride and dichlorodifluoromethane [25,26]. Pd-zeolites achieved higher selectivities to C2–C3 hydrocarbons than the Pt ones. It was concluded that the bond between carbon tetrachloride molecules and Pd atoms is stronger than with Pt. So, the probability of hydrogen insertion into the same carbon tetrachloride fragment is higher when using Pd than with Pt, resulting in more methane with Pt, and more ethane with Pd [26]. We have previously reported two studies about trichloromethane (TCM) conversion into C2–C3 hydrocarbons by catalytic hydrodechlorination with Pd supported on activated carbons obtained by the chemical activation of lignin [29,30]. These works concluded that the KOH-derived carbon catalyst achieved the best results in terms of selectivity to ethane and propane, with a selectivity to those compounds higher than 80% and a high dechlorination degree at 300 °C. However, Pd containing ZnCl₂- and FeCl₃-derived carbon catalysts yielded the best selectivity to olefins. Our research group has also compared catalytic HDC using different active phases supported on activated carbon using simulation and experimental analysis [31]. This study concluded that palladium yielded the best selectivity to C2–C3 hydrocarbons.

The purpose of this study is to analyze the effect of surface properties of Pd (1 wt.%) zeolite supported catalysts and reaction conditions in order to maximize the yield of valuable C2–C3 hydrocarbons by HDC of two model chloromethanes, namely, dichloromethane (DCM) and trichloromethane (TCM).

2. Results and Discussion

2.1. Characterization of the Catalysts

Figure 1 represents the nitrogen adsorption–desorption isotherms of the different catalysts at $-196\text{ }^{\circ}\text{C}$. According to IUPAC classification, HMOR and KL isotherms are of type I, with most of the N_2 uptake at low relative pressure and negligible hysteresis cycles, characteristics of microporous materials. On the other hand, the NaY catalyst showed type IV isotherm, characteristic of mesoporous materials with the presence of microporosity. The NaY isotherm presented the H4 hysteresis cycle associated with the capillary condensation of N_2 in the mesoporosity [32]. Furthermore, this catalyst showed the highest nitrogen adsorption capacities, and therefore, the most developed porous texture. The ionic exchange with ammonium resulted in a significant decrease in the amount of N_2 adsorbed, especially at low relative pressures, indicative of a reduction of the micropore volume. This reduction in porosity is a consequence of the cation interchange process, which according to inductively coupled plasma (ICP) results, reduced the amount of Na from 7.50% down to 0.22% for NaY and HY, respectively, and similarly reduced the K content from 11.81% down to 0.21% for KL and HL catalysts, respectively. These results agree with those previously reported by Sato et al. [33], who studied the structural changes of Y zeolites during ion exchange treatments, analyzing the effects of the initial Si:Al ratio of the zeolite. They concluded that at low Si:Al ratios of 2.4 (like that of the NaY zeolite used in our study) the zeolitic framework structure deteriorated during the successive ionic interchange steps, as evidenced by the reduction in the nitrogen adsorbed volume and crystallinity (as we will show later). Moreover, the lower reduction in the amount of nitrogen adsorbed in the ion-exchanged KL zeolite when compared to the NaY one can be due to the higher Si:Al ratio of the former. In general, the stability of the zeolitic framework during the ion exchange procedures decreased with increasing the number of Al in the framework [33].

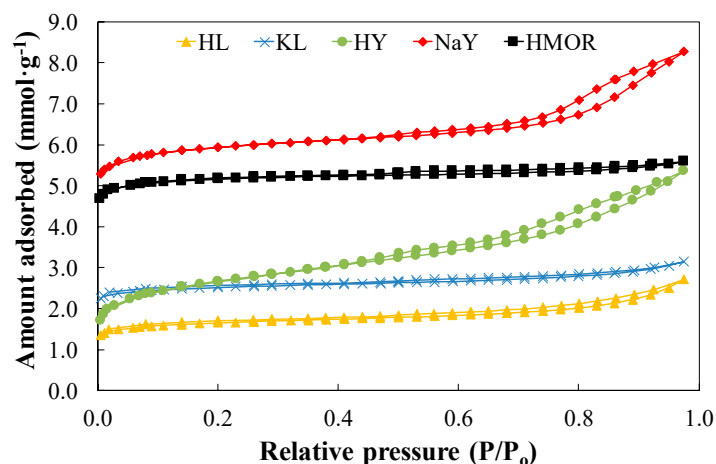


Figure 1. N_2 adsorption–desorption isotherms of the catalysts at $-196\text{ }^{\circ}\text{C}$.

Table 1 shows the surface area, A_{BET} , micropore area, A_{micro} , external surface area, A_{EXT} , and pore volume, V_{pore} , obtained from N_2 adsorption–desorption isotherms. All the catalysts showed moderate specific surface areas, ranging from 98 to $342\text{ m}^2\text{ g}^{-1}$, which are similar or slightly lower than those previously described in the literature [34–37]. Zeolites were impregnated with 1 wt.% of Pd, which could block a small part of the porosity of the zeolite support. The A_{BET} values confirm that those zeolites treated by ionic exchange, HY and HL, suffered a significant reduction of their porosity. After the ion exchange process, HY showed an A_{BET} reduction close to 50%, very similar to the reduction reported by Sato et al. [33] for the NaY zeolite with same Si/Al ratio after three cycles of ion exchange. This indicates the deterioration of the zeolitic framework structure, which was corroborated later by X-ray diffraction analyses (XRD). Table 2 shows the Pd concentrations of the catalysts determined by

ICP. As can be seen, the amounts of Pd in the different catalysts were very close to the selected 1 wt.%, confirming the successful incipient wetness impregnation.

Table 1. Characteristic parameters of the porous texture of the catalysts.

Catalyst	A_{BET} ($\text{m}^2 \text{g}^{-1}$)	V_{micro} ($\text{cm}^3 \text{g}^{-1}$)	A_{EXT} ($\text{m}^2 \text{g}^{-1}$)	V_{pore} ($\text{cm}^3 \text{g}^{-1}$)
KL	145	0.075	28	0.109
NaY	342	0.177	67	0.287
HMOR	293	0.164	34	0.194
HL	98	0.043	33	0.094
HY	174	0.041	59	0.186

Table 2. Pd mean particle size and dispersion from TEM, total desorbed ammonia obtained from TPD-NH₃ and Pd metal mass content from ICP.

Catalysts	TEM		NH ₃ -TPD	ICP
	Mean Pd Particle Size (nm)	Dispersion (%)	Desorbed NH ₃ (mmol g^{-1})	Pd (%)
KL	6.3	18	0.37	1.02
NaY	4.2	26	1.49	0.97
HMOR	1.9	57	2.29	0.98
HL	1.4	79	1.75	0.99
HY	2.3	48	1.96	1.03

Figure 2 shows the temperature programmed reduction (TPR) profiles of the non-reduced catalysts. The evolution of Pd species upon H₂-TPR is well-described in the literature [38,39]. Bulk PdO reduces in H₂ atmosphere at room temperature (around 25 °C or even lower) and forms palladium hydrides, β -PdH_x [40]. In our experimental set-up, we assumed that all the accessible PdO was reduced during the initial step of the TPR at 30 °C for 30 min in the H₂ mixture before the heating up. Subsequently, reduced Pd formed palladium hydrides. When heating began, these hydrides decomposed at higher temperatures as negative peaks in the H₂-TPR profiles. Position and intensity of the peaks are related to the size and dispersion of supported Pd metal. Bigger accessible particles show higher storage capacities than the smaller ones, showing clear negative peaks at low temperatures. In contrast, in smaller Pd particles the decomposition of β -PdH_x occurs at higher temperatures [41]. The H₂-TPR profiles of NaY and KL catalysts clearly showed the presence of negative peaks at temperatures of 107 °C and 80 °C, respectively, indicative of the presence of larger Pd particles, which have a greater capacity for hydride formation and therefore give a negative peak of H₂ desorption when the temperature increases. These negative peaks were not observed in HMOR or interchanged zeolites HY and HL, which suggests that these catalysts present smaller palladium particles. These facts were corroborated further in this study by the analysis of the palladium particles sizes by TEM. Further increase of the reaction temperature produced the reduction of the oxides, with the consequent positive peaks in the H₂-TPR profiles. As can be seen, most of the more intense peaks in the profiles were located between 120 °C and 200 °C, although there were also other peaks at higher reduction temperatures, between 350 °C and 450 °C. The peaks at lower reduction temperatures are associated with the reduction of the oxides of Pd located inside cavities of the zeolite of good accessibility, while those at higher temperatures are related to the reduction of the oxides in places of more difficult access, like subsurface PdO species [42,43]. It is noticeable that the patterns at lower reduction temperature suggest the presence of two different Pd phases. KL showed a single peak displaced at slightly higher temperatures than those of ion-exchanged zeolites, while NaY showed both phases. The higher and only presence of the phase in the KL pattern around 170 °C, in comparison with NaY, may indicate a higher interaction of Pd with the zeolitic support. This phase can be related not only with the Pd species formed, but also with the localization of these Pd particles in the zeolitic structure. The position

and accessibility of this phase can represent relevant differences in the catalytic activity and selectivity distribution, as was observed further in this study. On the basis of TPR results, it can be concluded that the reduction temperature of 400 °C is sufficient to reduce the Pd species in the catalysts.

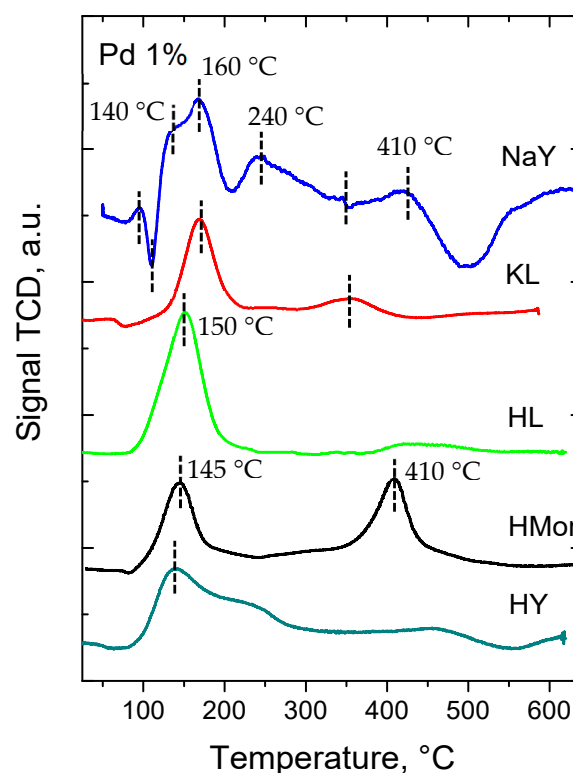


Figure 2. TPR-H₂ profiles of the different catalysts in 4.8% H₂/Ar, 10 °C/min.

XRD patterns of the five catalysts are represented in Figure S1 in the Supplementary Information. The main reflections of mordenite in the HMOR patterns were identified at 9.6°, 13.4°, 25.6°, and 27.7°, corresponding to (2 0 0), (1 1 1), (2 0 2), and (5 1 1) planes, respectively [44,45]. KL and HL showed characteristic diffraction peaks at 5.5°, 11.8°, 15.2°, 19.3°, 22.7°, 28.0°, and 30.7°, associated with (1 0 0), (0 0 1), (1 1 1), (2 2 0), (2 2 1), and (2 1 2) planes, respectively [46,47]. Finally, the main diffraction peaks associated with NaY and HY zeolites were confirmed by the peaks at 6.3°, 10.3°, 12.1°, 15.9°, 23.5°, 26.9°, and 31.3° corresponding to (1 1 1), (2 2 0), (3 1 1), (3 3 1), (5 3 3), (6 4 2) and (5 5 5) planes, respectively [33,37,48]. As can be seen, all the samples showed well-defined diffraction peaks, confirming the high crystallinity of the zeolites. Despite this, certain differences were found between the exchanged and the non-exchanged zeolites. The ammonium exchanged zeolites, HL and HY, showed lower crystallinity and a slight shift in the diffraction peaks in relation to those of the non-exchanged zeolites, KL and NaY, respectively. These results support those previously obtained when analyzing the nitrogen adsorption–desorption isotherms. After three cycles of ion exchanges the porous texture was affected by the removal of the compensating cation (Na in NaY and K in KL) out of the zeolite, causing a deterioration of the zeolitic framework, resulting in a lower porosity, as indicated in N₂ isotherm analysis, and corroborated by the loss of crystallinity observed by XRD. These results are in agreement with those reported in the literature [33,46]. It is also worth mentioning that Pd diffraction peaks were not observed in any of the zeolite spectra. This suggests that Pd particles should be of relatively low size and therefore a high dispersion was obtained, as confirmed below by TEM results.

Figure 3 displays representative TEM images of the different catalysts and their Pd particle size distributions. The images show Pd particles of different sizes depending on the catalysts, with quasi-spherical shape and relatively good homogeneous distribution. Non-exchanged zeolites, KL

and NaY, resulted in catalysts with the most heterogeneous particle size distributions, even more heterogeneous in the case of KL catalysts. In contrast, exchanged zeolites, HL and HY, resulted in catalysts with a very homogeneous particle size distribution with lower mean size. HMOR catalysts also showed a homogeneous particle size distribution. Table 2 reports Pd mean particle size and dispersion values obtained from TEM analysis. The highest mean Pd particle sizes were those of KL and NaY catalysts (6.3 nm and 4.2 nm, respectively), while the rest of the catalysts showed similar mean sizes in the range 1.4–2.3 nm.

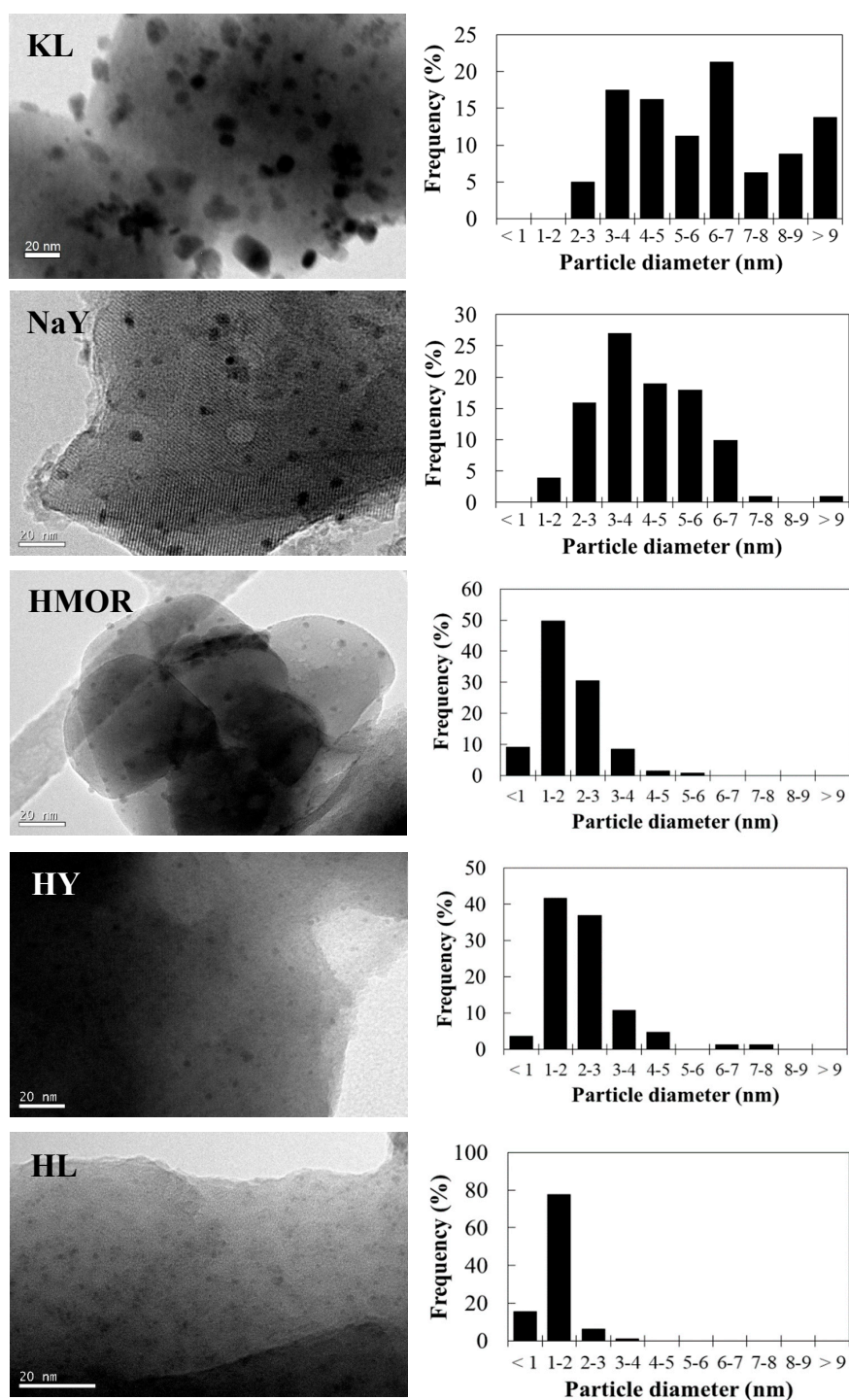


Figure 3. Pd-particle size distribution of the catalysts.

The different values of mean particle size can be explained by the surface acidity of the zeolites, which was analyzed by temperature programmed desorption of ammonia (NH₃-TPD). Figure 4 depicts the NH₃-TPD profiles of the five different catalysts. The desorption temperature of the peaks and their intensity can be associated with the strength and number of the acidic sites, respectively. The KL catalyst had the lowest acidity, with only one low intensity peak at 210 °C associated with low-strength acid sites. This catalyst also showed the biggest mean particle size (6.3 nm), which was around five times the mean particle size of HL catalyst (1.4 nm). NaY and HY followed the same tendency, showing a higher particle size than non-exchanged zeolite (4.2 nm), although the difference between these two catalysts was lower. According to NH₃-TPD results, NaY desorption peaks were more intense below 400 °C, showing a higher number of acid sites but still weak. On the contrary, HY and HL showed higher acidity according to their desorption profiles, and both samples showed the presence of acid sites that desorbed at higher temperatures than 400 °C (stronger acid sites). It seems clear that higher acidity yields Pd particles with smaller size. HMOR showed the highest acidity of the five catalysts, identified by the presence of intense peaks of NH₃ desorbed at 200 °C, 550 °C, and 775 °C, related to the presence of acid sites of heterogeneous strength. Table 2 summarizes the total desorbed ammonia obtained from TPD-NH₃ spectra by integration of the area under the curve. The surface acidity of the five catalysts followed the order HMOR > HY > HL > NaY > KL. With the objective of clarifying the relationship between Pd particle size and catalyst acidity, Figure 5 represents the total amount of NH₃ desorbed by the catalysts during the NH₃-TPD tests versus Pd mean particle size obtained from TEM. The correlation between acidity and particle size is clearly visible. The catalysts with higher surface acidity yielded lower mean Pd particle sizes. This behavior has been already observed in the literature for Pd on different supports, and it is ascribed to different reasons, such as reduction of pore volume and surface area and hindering of anchorage of the Pd precursor [29,49]. These results are also in agreement with the TPR results, where non-exchanged catalysts showed lower hydride capacity due to their smaller Pd particle size.

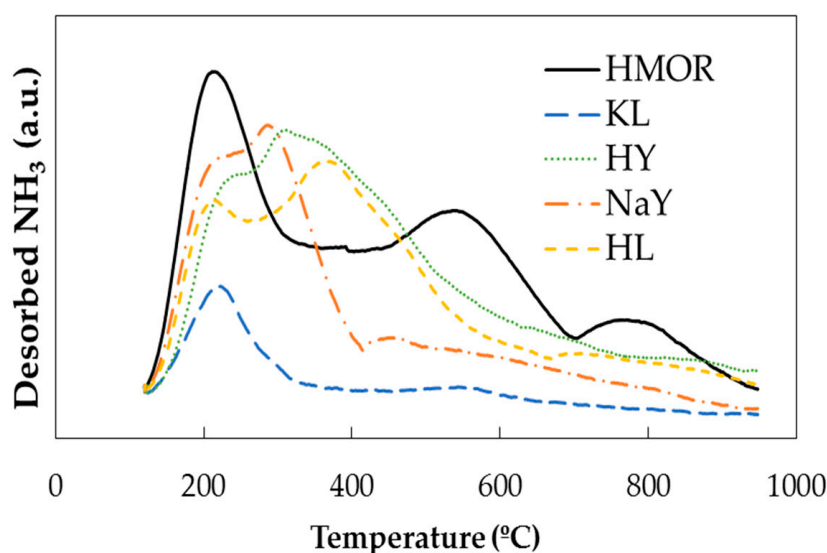


Figure 4. NH₃-TPD curves of the catalysts.

The Pd external mass content and the oxidation state distribution were studied by X-ray photoelectron spectroscopy (XPS). Table 3 displays the Pd mass surface concentration. It can be observed that in all the catalysts the external surface concentration of Pd was significantly lower than the bulk one (1% Pd). This indicates that the Pd was more concentrated in the interior of the support particles (“egg-yolk” distribution). In the Pd3d XPS regions the doublet corresponding to Pd 3d_{5/2} and Pd 3d_{3/2} was visible, separated by 5.26 eV [50]. The Pd 3d_{5/2} signal at 335.5 eV was assigned to metallic palladium (Pd⁰), while electro-deficient palladium (Pdⁿ⁺) appeared around at 338.0 eV [19,29]. Table 3 represents the Pd3d oxidation state distribution obtained from Pd3d XPS spectra deconvolution (Figure S2). In all the cases, the catalysts showed predominantly Pd in the metallic state as a consequence of the reduction step in H₂.

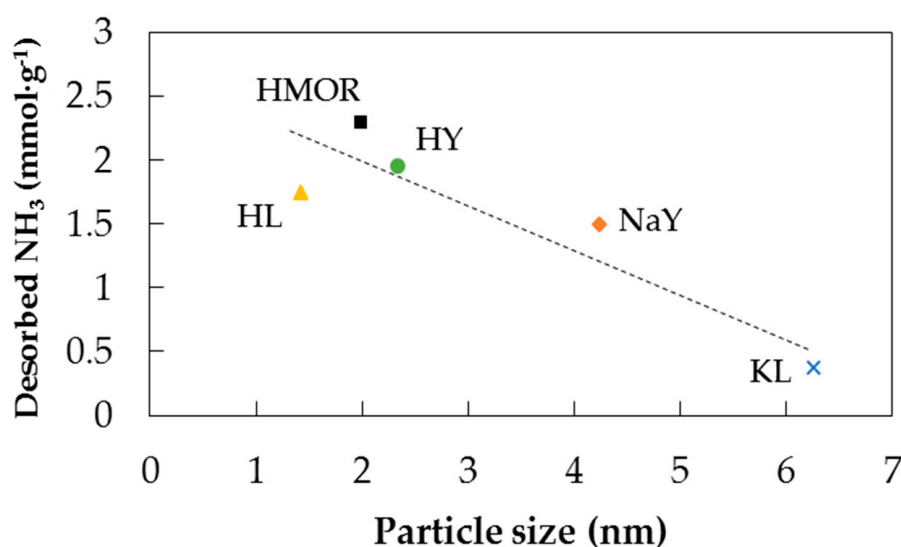


Figure 5. Desorbed NH₃ versus Pd mean particle size.

Table 3. Pd external mass content, Pd⁰ and Pdⁿ⁺ obtained from XPS.

Catalyst	Pd External Mass Content (%)	Pd ⁰ (%)	Pd ⁿ⁺ (%)
KL	0.38	72	28
NaY	0.67	95	5
HMOR	0.55	85	15
HL	0.27	87	13
HY	0.11	87	13

2.2. HDC Tests

Figure 6a,b represent the initial DCM and TCM conversion, respectively, with reaction temperature using the five catalysts. All the catalysts showed significant activity on the HDC reaction with conversions of both DCM and TCM increasing with reaction temperature. In the case of HDC of DCM (Figure 6a), the KL catalyst showed the lowest conversion values (≈40% at 300 °C), probably as a consequence of its higher Pd mean particle size. On the contrary, the HMOR catalyst drove the highest DCM conversion values. This high activity can be explained by the combination of different characteristics, such as a well-developed porous texture, high surface acidity, and low Pd mean particle size. DCM conversion using NaY, HL, and HY catalysts was very similar along the whole reaction temperature range, which can be explained by the similarities found in their total surface acidity. The activity of the catalysts in the HDC of DCM seemed to follow the same order as the total surface acidity. This behaviour has been previously observed for other reactions on zeolite catalysts [51]. On the other hand, the HDC of TCM showed higher conversion values than DCM with all the catalysts. This is due to the higher reactivity of the TCM molecule, as a consequence of the additional Cl atom in the

chloromethane molecule. In this case, total conversion of TCM was reached at a lower temperature (175 °C) with HY, NaY, and HMOR catalysts. Like in the case of DCM, KL showed the lowest conversion values, probably due to its higher Pd particle sizes.

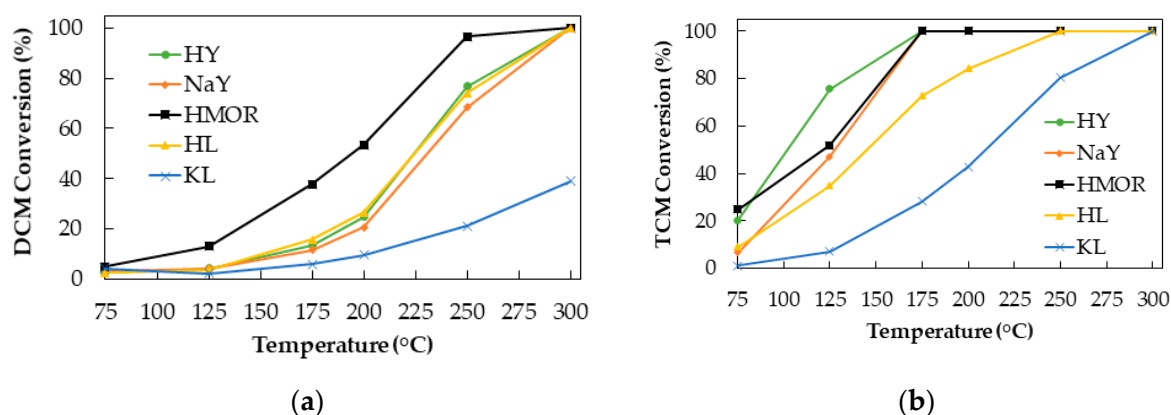


Figure 6. DCM (a) and TCM (b) conversion versus reaction temperature with the different catalysts ($\tau = 0.8 \text{ kg h mol}^{-1}$, $\text{H}_2/\text{Chloromethane}$: H_2/CM molar ratio = 100).

To establish more clearly the possible influence of Pd particle size on the conversion of DCM and TCM with all the catalysts, Figure 7 depicts the turnover frequency (TOF) values at isoconversion ($X = 50\%$) versus particle size for the HDC of TCM and DCM. The HDC of TCM and DCM appears to be a structure-sensitive reaction, with activity increasing with the Pd particle size. We have observed a similar behavior when analyzing the HDC of TCM using Pd supported on activated carbons catalysts at similar reaction conditions [29]. Taking into account the good correlation between TOF values and Pd mean particle size (Figure 7), it seems that the different nature of the catalytic sites (with different reduction temperatures, as can be seen in Figure 2) has lower significance in the HDC behavior using the different catalysts. Bonarowska et al. [15] reported TOF values on the HDC of tetrachloromethane in the range of 25–1650 h^{-1} at 90 °C, with silica- and alumina-supported Pt catalysts. This research group also reported TOF values in the range of 7.3–619 h^{-1} with Pd, Au, and Au-Pd on Sibunit carbon catalysts [52]. Sánchez et al. [53] reported TOF values of 0.9 h^{-1} at 120 °C on the HDC of DCM using alumina and sol-gel titania-supported Pd catalysts. Ramos et al. [49] obtained TOF values of around 10,080 h^{-1} for the HDC of TCM at 100 °C and a H_2/TCM ratio of 12. Pt-Pd bimetallic particles supported on sulfate zirconia catalysts showed TOF values in the range of 25.2–75.6 h^{-1} in the HDC of DCM at 150 °C [54]. Similar results to our work were obtained also by Martin-Martinez et al. [55], where TOF values were in the range of 98–1173 h^{-1} between 125 and 250 °C, using Pd supported on carbon material.

The main purpose of this work was not only the treatment of chloromethanes, but also the transformation into valuable hydrocarbon products, such as light olefins and paraffins. With this objective, we studied the selectivity distribution of the different reaction products. Figures S3 and S4 represent the evolution of selectivity with the reaction temperature for all the catalysts, on the HDC of DCM and TCM. The reaction products obtained were methane, ethane, and propane, accompanied by monochloromethane (MCM) and dichloromethane (DCM), as result of incomplete hydrodechlorination of the reactants. Significant production of propane was only observed in the HDC of TCM, while very small amounts of partially-chlorinated compounds were found for this reaction. Traces of ethylene were also detected with the KL catalyst. In the HDC of DCM (Figure S3) at low temperatures, the main product obtained with all the catalysts was methane. As reaction temperature increased (and therefore DCM conversion increased) a very significant reduction in the selectivity to MCM was observed, accompanied by increasing selectivities to the desired products, the light paraffins ethane and propane. Furthermore, in the case of KL catalysts, ethane was the main reaction product of HDC of DCM at 300 °C. It is worth mentioning the high dechlorination degree of the catalysts, indicated by the low

selectivity obtained for MCM at high temperatures (when the DCM conversion begins to be significant). The selectivities in the HDC of TCM (Figure S4) followed similar trends, although some differences should be pointed out. Higher selectivities to the light paraffins (ethane and propane) than in the HDC of DCM were obtained, favored at the highest temperatures analyzed. Ethane was the main reaction product at reaction temperatures equal to or higher than 250 °C with all the catalysts. Propane selectivity was significantly higher in the HDC of TCM than DCM. High dechlorination degree was also obtained in the HDC of TCM with all the catalysts, with total amounts of MCM + DCM even lower than those of MCM alone in the HDC of DCM.

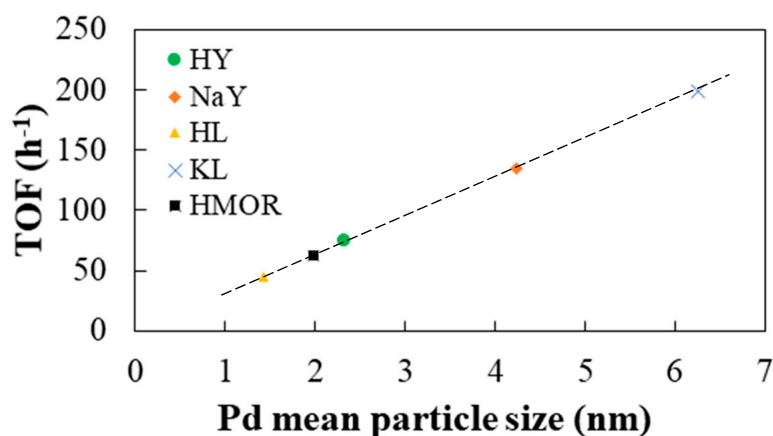


Figure 7. Turnover frequency (TOF) (50% conversion) versus mean particle size for the hydrodechlorination (HDC) of DCM and TCM.

Figure 8a,b represent the selectivity distribution for the different reaction products in the HDC of DCM and TCM, respectively, at 300 °C. In the HDC of DCM (Figure 8b) HY, NaY, and HL showed similar selectivities to the different products, with ethane and propane selectivities around 33%, and high dechlorination (selectivity to MCM < 6%). The HMOR catalyst showed the lowest selectivity to ethane and propane (around 17%) and the highest selectivity to methane (78%). In contrast, the KL catalyst showed the highest selectivity to the preferred products (selectivity to ethane and propane around 60%), and the lowest selectivity to methane, around 38%. As can be seen in Figure 8a, the HDC of TCM yielded significantly higher selectivities to ethane and propane than the HDC of DCM, with also very high dechlorination degrees (low selectivities to DCM and MCM). The NaY and KL catalysts showed the most promising results, with selectivities to ethane and propane of 82% and 84%, respectively. In a general trend, it can be seen that the KL catalyst, with the lowest surface acidity, showed the lowest conversion values but the best results in terms of selectivity to ethane and propane in the HCD of both DCM and TCM. In contrast, the HMOR catalyst, which had the highest and strongest surface acidity, showed very high conversion values but the lowest selectivities to ethane and propane. These results suggest that surface acidity has an enormous effect not only in the activity but also in the selectivity of the HDC reaction. We obtained similar conclusions when analyzing the HDC of TCM using Pd on activated carbon catalysts [29]. In that study, the most acid catalyst, prepared from lignin by chemical activation with phosphoric acid, also yielded the lowest selectivities to ethane and propane. Comparing the results of both studies (this work with zeolites and the previous one with activated carbons), the highest selectivities to ethane and propane were very similar at 300 °C.

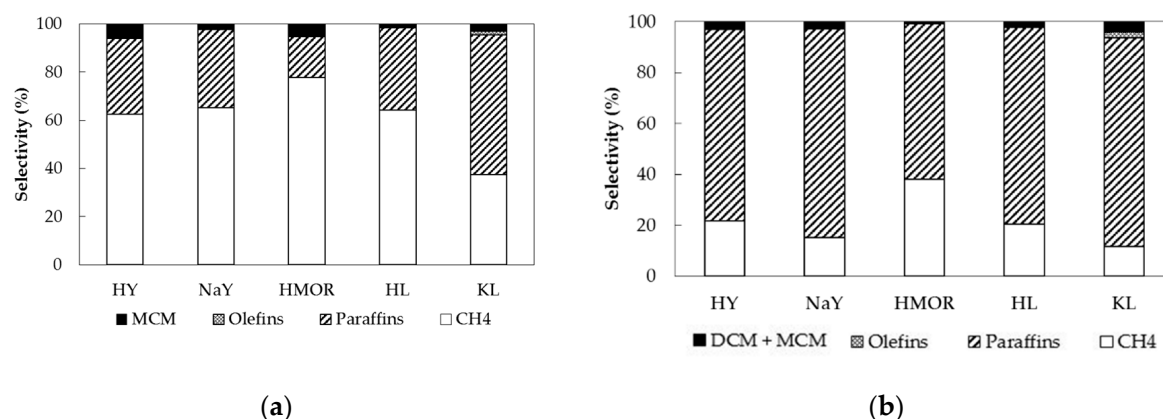


Figure 8. Selectivity distribution in the HDC of DCM (a) and TCM (b) with the different catalysts (reaction temperature = 300 °C, $\tau = 0.8 \text{ kg h mol}^{-1}$, H_2/CM molar ratio = 100).

Hydrogen concentration has been reported to have a substantial impact on the selectivity of the HDC reaction [30]. Decreasing the $\text{H}_2:\text{CM}$ ratio generally increases the selectivity to olefins, although it can also reduce the chloromethanes conversion and even reduce the stability of the catalyst. Figure 9a,b depict conversion and selectivity distribution in the HDC of DCM and TCM, respectively, with NaY and KL catalysts at $\text{H}_2:\text{CM}$ ratios of 10 and 100. We selected these catalysts because they showed the highest selectivities to light paraffins (ethane and propane). The conversion values decreased slightly when reducing the H_2/DCM molar ratio from 100 to 10. Regarding the effect of the H_2/CM ratio on the selectivity values, it can be clearly observed that a reduction of the $\text{H}_2:\text{CM}$ ratio significantly enhances the selectivity towards light hydrocarbons, paraffins, and in the case of KL catalysts, olefins (ethylene and propylene). NaY catalysts produced outstanding selectivities to paraffins in the HDC of DCM and TCM (around 70% and 95%, respectively) when using the lower H_2/CM ratio. In the case of KL catalysts, a clear increase in the selectivity to C2–C3 hydrocarbons was also observed with a very significant proportion of olefins, especially in the HDC of TCM, reaching a selectivity to olefins close to 60%. However, this latter excellent result was negatively affected by the high selectivity to chloromethanes (22%) as incomplete dechlorination by-products. Slightly lower selectivity to chlorinated products was obtained with NaY catalysts, confirming that more and smaller active sites enhance the hydrodechlorination capability of the catalysts.

The use of higher reaction temperatures (up to 400 °C) was also analyzed for the HDC of DCM at a $\text{H}_2:\text{DCM}$ molar ratio of 10 using both catalysts—NaY and KL. Despite better results being obtained in terms of conversion and selectivities (selectivities to olefins 75% with KL), the carbon balance in the reaction failed by 20%. This carbon shortage was probably caused by the generation and adsorption of condensation by-products on the surface of the catalysts, which decrease olefin yields and provoke the deactivation of the catalysts.

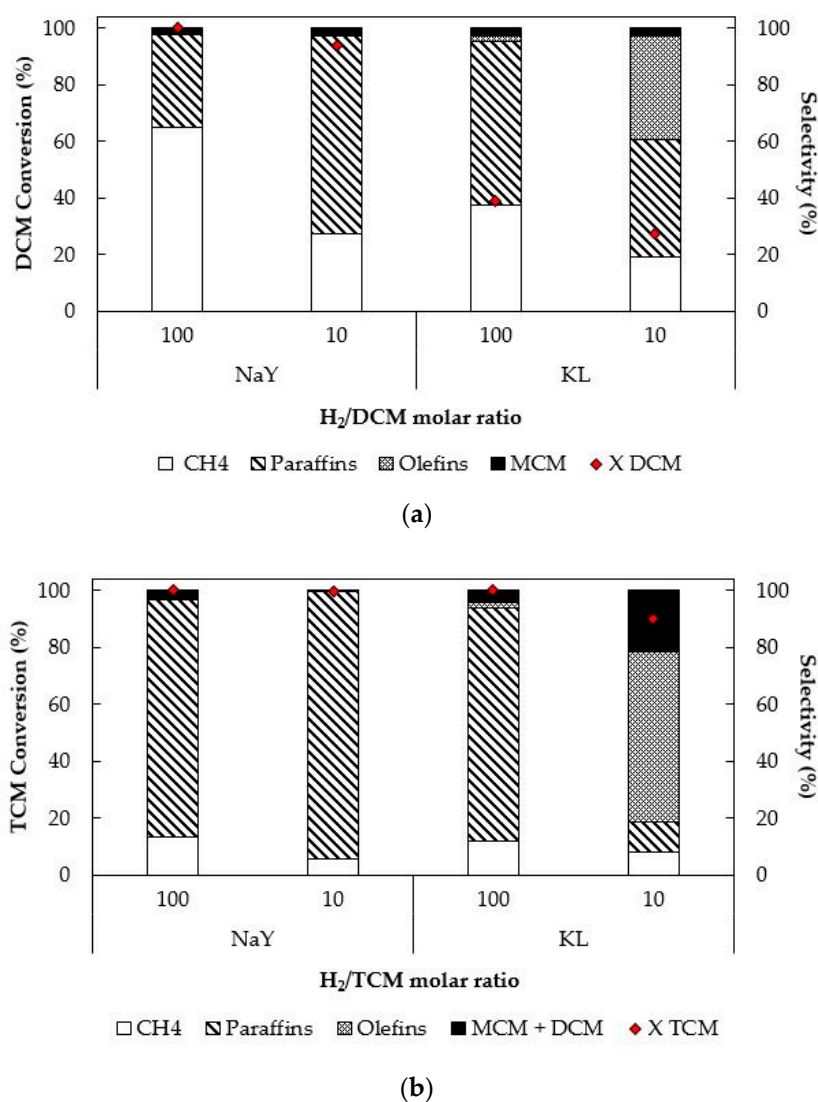


Figure 9. Conversion and selectivity distribution in the HDC of (a) DCM and (b) TCM with NaY and KY catalysts at H₂:CM ratios of 10 and 100 (reaction temperature = 300 °C, $\tau = 0.8 \text{ kg h mol}^{-1}$).

3. Materials and Methods

3.1. Materials and Chemicals

Three commercial zeolites were used in the preparation of the catalysts, namely K-LTL, Na-Y, and H-MOR. The K-LTL (Lynde Type L) zeolite has a three-dimensional channel distribution with a composition of $\text{K}_6\text{Na}_3\text{Al}_9\text{Si}_{27}\text{O}_{72} \cdot 21\text{H}_2\text{O}$ (SK-45, Si/Al = 3), and was purchased from Union Carbide (Houston, TX, USA). The NaY zeolite (Faujasite type) has a three-dimensional channel distribution and a composition of $(\text{Na}_2)_{3.5}[\text{Al}_7\text{Si}_{17}\text{O}_{48}] \cdot 32\text{H}_2\text{O}$ (Si/Al = 2.4, UOP-Y 54), and was purchased from Universal Oil Products (Des Plaines, IL, USA). Finally, the H-MOR zeolite (Mordenite) has a two-dimensional channel distribution, its composition is $\text{H}_2[\text{Al}_2\text{Si}_{10}\text{O}_{24}] \cdot 7\text{H}_2\text{O}$ (Si/Al = 7, Zeolon 900 H), and it was obtained from Norton International. PdCl₂ (99.9%), used as the active phase precursor, was supplied by Sigma-Aldrich (St. Louis, MO, USA). All the gases were supplied by Praxair (Pinto, Madrid, Spain): trichloromethane (0.15% vol. in N₂), dichloromethane (1.5 % vol. in N₂), H₂, and N₂ (both 99.999% purity).

3.2. Synthesis of the Catalysts

All zeolites were initially calcined, prior to use, in a vertical quartz reactor under dry air flow (60 mL min^{-1}) at $450 \text{ }^\circ\text{C}$ (heating rate $5 \text{ }^\circ\text{C min}^{-1}$) for 4 h. In order to obtain catalysts with different chemical properties, K-LTL and Na-Y supports were submitted to ion exchange steps. Five grams of the calcined zeolites were dispersed in 100 mL of 1 M NH_4NO_3 solution under stirring at $90 \text{ }^\circ\text{C}$ for 6 h. The solid was recovered by filtration, washed with distilled water, dried in an oven overnight, and calcined again in the same previous conditions. The operation was repeated three times to ensure the correct ion exchange between Na^+/K^+ cations and NH_4^+ . During calcination, NH_4^+ was decomposed into H^+ and NH_3 was released.

Subsequently, Pd was added as active phase on the zeolite by the incipient wetness impregnation method. Aqueous solutions of PdCl_2 with adjusted concentrations to achieve a Pd bulk concentration of 1% in weight were prepared and deposited dropwise on the dried zeolite supports. After impregnation, the catalysts were dried at room temperature for 24 h, and later dried in an oven. Finally, the resulting catalysts were calcined again at $450 \text{ }^\circ\text{C}$ in air (60 mL min^{-1}) for 4 h. The obtained catalysts impregnated with Pd (1 % wt) were identified as HL (K-LTL interchanged with NH_4^+), KL (K-LTL zeolite), NaY (Na-Y zeolite), HY (Na-Y interchanged with NH_4^+), and HMOR (H-MOR zeolite).

3.3. Characterization

All catalysts were reduced prior to any characterization (except for TPR analyses). The reduction was performed at $400 \text{ }^\circ\text{C}$ for 1 h under H_2 atmosphere (100 mL min^{-1}). The porous texture of the catalysts was studied by N_2 adsorption–desorption at $-196 \text{ }^\circ\text{C}$ on an ASAP 2020 equipment (Micromeritics, Norcross, GA, USA). All the samples were previously outgassed at $200 \text{ }^\circ\text{C}$ under vacuum (10^{-6} Torr) for 6 h. The BET equation was used to calculate the specific surface area; meanwhile, the t-method was used to find the external surface area and micropore volume. Total pore volume was quantified by the N_2 at $P/P_0 = 0.99$, transformed in liquid volume (V_{pore}). Crystalline structure was studied by X-ray powder diffraction (XRD) and performed on a PANalytical X'Pert PRO diffractometer (Malvern, Worcestershire, UK). The powdered samples were analyzed using $\text{CuK}\alpha$, voltage of 45 kV, and current 40 mA. The scanning range of $2\theta = 4\text{--}90^\circ$ was set up, with a scan step size 0.04 rad and 20 s counting time.

The acidity of the catalysts was analyzed in an Autochem II 2920 apparatus (Micromeritics, Norcross, GA, USA) by temperature-programmed desorption of ammonia (NH_3 -TPD). The catalysts (0.190 g) were saturated with 25 mL min^{-1} of 5% NH_3/He at $100 \text{ }^\circ\text{C}$. Subsequently, the feebly adsorbed NH_3 was desorbed in helium flow (25 mL min^{-1}) at the same temperature, until no outlet of NH_3 was detected. The NH_3 -TPD was obtained by increasing the temperature up to $940 \text{ }^\circ\text{C}$ ($10 \text{ }^\circ\text{C min}^{-1}$). The NH_3 desorbed was monitored with a thermal conductivity detector (TDC). Temperature-programmed reduction (TPR) analyses were carried out on an Ohkura TP2002 equipment (Sakado, Saitama, Japan) using also a thermal conductivity detector. The non-reduced catalyst (0.1 g) was situated in a quartz tube and under dry air (20 mL min^{-1}) at $450 \text{ }^\circ\text{C}$ for 1 h and then cooled down to room temperature. Afterwards, a mixture of H_2 (4.8%) with Ar was passed (20 mL min^{-1}) at $30 \text{ }^\circ\text{C}$ for 30 min. Then, the temperature was increased up to $650 \text{ }^\circ\text{C}$ at $10 \text{ }^\circ\text{C min}^{-1}$ and maintained for 30 min. Chemical analyses were performed by inductively coupled plasma (ICP) on an ICP-OPTIMA 2100 DV-Perkin Elmer (Waltham, MA, USA). The solid samples were digested on microwave by using proper acid mixture solution.

X-ray photoelectron spectroscopy (XPS) was performed in a Thermo Scientific with Al $\text{K}\alpha$ radiation (1486.7 eV). The wide spectra were acquired by scanning binding energy (BE) in the 0–1200 eV range. The C1s peak (284.6 eV) was considered as an internal standard and used for corrections of changes occurring in BE caused by sample charging. The morphologies and size distribution of the Pd particles were studied by transmission electron microscopy (TEM). The micrographs were acquired with a JEM 2100 microscope (JEOL, Akishima, Tokyo, Japan) at 200 kV of accelerating voltage. At least 100 particles were measured for the particle size distribution analysis.

3.4. Gas-Phase HDC Tests

All the tests were carried out in a continuous flow Micro-Activity equipment (PID Eng & Tech, Alcobendas, Madrid, Spain), described elsewhere [11], with a quartz microreactor (4 mm). Initially, the sample were in situ reduced in a H₂ atmosphere (50 mL min⁻¹) at 250 °C for 2 h prior to any reaction test. The HDC experiments were performed at atmospheric pressure, with 100 mL min⁻¹ of total flow (TCM/DCM + N₂ + H₂), a TCM/DCM inlet concentration of 1000 ppmv, space time of $\tau = 0.8 \text{ kg h mol}^{-1}$, different H₂:TCM/DCM molar ratios (100:1–10:1 range), and reaction temperatures from 75 to 300 °C. The reactor exit was connected to a gas chromatograph (Varian 450-GC) equipped with a capillary column (CP-SilicaPLOT, 60 m) and an FID detector. The activity of the catalysts was evaluated, quantifying TCM and DCM conversion (X), and the selectivity to the different products (S_i) was determined by:

$$X_{\text{TCM}} (\%) = (\text{TCM}_{\text{inlet}} - \text{TCM}_{\text{outlet}}) / \text{TCM}_{\text{inlet}} \times 100,$$

$$X_{\text{DCM}} (\%) = (\text{DCM}_{\text{inlet}} - \text{DCM}_{\text{outlet}}) / \text{DCM}_{\text{inlet}} \times 100,$$

$$S_i (\%) = (n_i^{\text{outlet}} N_{C,i}) / (n_i^{\text{outlet}} N_{C,i} + n_j^{\text{outlet}} N_{C,j} + \dots) \times 100,$$

where n_i^{outlet} and n_i^{inlet} are the concentration of the product *i* at the reactor exit and inlet, respectively, $N_{C,j}$ and $N_{C,i}$ are the number of carbon atoms in the compounds *j* and *i*, respectively. The carbon mass balance of every experiment was checked and did not showed deviations higher than 10%. Turnover frequency (TOF) was also evaluated and calculated as the moles of reactants converted per mole of surface-exposed active phase atoms (Pd atoms). Dispersion of Pd particles was estimated, supposing a spherical shape, utilizing the equation [29]:

$$D (\%) = (6 \cdot 10^5 M_w) / (\rho_M \sigma_M N_A d),$$

where M_w stands for the Pd atomic mass (106.42 g mol⁻¹), ρ_M is the density of the metal (12.02 g cm⁻³ for Pd), σ_M corresponds to the effective surface area of Pd atoms (7.87 × 10⁻²⁰ m² per atom), N_A is Avogrado's number, and *d* is the mean metal particle size (obtained by TEM) in nm. The number of metal atoms exposed was estimated using the bulk Pd content (μmol per gram) multiplied by the dispersion values.

4. Conclusions

Pd supported by incipient wetness impregnation on commercial zeolites type K-LTL, Na-Y, and Na-MOR, synthesized in basic form or modified to protonic by ion exchange with ammonium, resulted in catalysts with good performance in the HDC of DCM and TCM. The ion exchange process allowed the modification of surface acidity, porosity, and Pd particle size. The catalysts with higher surface acidity yielded lower mean Pd particle size, which in turn reduced the intrinsic activity of the catalysts. This confirmed the HDC of TCM and DCM as a structure-sensitive reaction. The best results in terms of selectivity to the desired products (C2–C3 hydrocarbons) were obtained with NaY and KL catalysts, due to their lower surface acidity. The NaY catalyst showed a total conversion of both DCM and TCM, with selectivities to paraffins of 70% and 95%, respectively. In the case of the KL catalyst, the conversion achieved with DCM was significantly lower (around 27% at 300 °C), and a higher temperature was needed to obtain complete TCM conversion, although with excellent selectivities to C2–C3 hydrocarbons. Surface acidity had an outstanding influence on the selectivity to olefins. KL catalysts, with a considerably lower acidity than the other catalysts, led to selectivities to olefins up to 37% and 60% for DCM and TCM HDC, respectively. In contrast, NaY did not produce significant amounts of olefins. Catalysts with low surface acidity are recommended for getting high selectivities of C2–C3 hydrocarbons by HDC of chloromethanes, and especially to yield olefins.

Supplementary Materials: The following are available online at <http://www.mdpi.com/2073-4344/10/2/199/s1>, Figure S1: XRD patterns of the catalysts, Figure S2: XPS Pd3d deconvoluted spectra Pd 1%, Figure S3:

Selectivity versus reaction temperature on the HDC of DCM with the catalysts ($\tau = 0.8 \text{ kg}_{\text{cat}} \text{ h mol}^{-1}$, 1000 ppmv, $\text{H}_2/\text{DCM} = 100$), Figure S4: Selectivity versus reaction temperature on the HDC of TCM with the catalysts ($\tau = 0.8 \text{ kg}_{\text{cat}} \text{ h mol}^{-1}$, 1000 ppmv, $\text{H}_2/\text{TCM} = 100$), Table S1: XPS analysis of the fresh catalysts at high resolution.

Author Contributions: Conceptualization, J.B., J.J.R. and L.M.G.-S.; methodology, C.F.-R., J.B., J.M.G. and L.M.G.-S.; data analysis, C.F.-R., J.B., J.M.G., D.R. and L.M.G.-S.; investigation, C.F.-R., J.B., D.R., A.C.R. and L.M.G.-S.; writing—original draft preparation, C.F.-R.; writing—review and editing, C.F.-R., J.B., L.M.G.-S. and J.J.R.; supervision, J.B., J.M.G., J.J.R. and L.M.G.-S. All authors have read and agreed to the published version of the manuscript.

Funding: Authors gratefully acknowledge financial support from FEDER/Ministerio de Ciencia, Innovación y Universidades—Agencia Estatal de Investigación/CTM2017-85498-R. C. Fernández Ruiz acknowledges MINECO for his research grant.

Conflicts of Interest: The authors declare no conflict of interest.

References

1. Huang, B.; Lei, C.; Wei, C.; Zeng, G. Chlorinated volatile organic compounds (Cl-VOCs) in environment—Sources, potential human health impacts, and current remediation technologies. *Environ. Int.* **2014**, *71*, 118–138. [[CrossRef](#)] [[PubMed](#)]
2. Kurylo, M.J.; Rodriguez, J.M.; Andrae, M.O.; Atlas, E.L.; Blake, D.R.; Butler, J.H.; Lal, S.; Lary, D.J.; Midgley, P.M.; Montzka, S.A.; et al. *Scientific Assessment of Ozone Depletion: 2014*; WMO: Geneva, Switzerland, 2014; ISBN 9789966076014.
3. Zhao, J.; Chen, M. Leak Detection and Repair (LDAR) Standard Review for Self-Inspection and Management for VOC Emission in China's Traditional Energy Chemical Industry. *J. Environ. Prot.* **2018**, *9*, 1155–1170. [[CrossRef](#)]
4. Fraas, A.G.; Egorenkov, A. A Retrospective Study of EPA's Rules Setting Best Available Technology Limits For Toxic Discharges to Water Under the Clean Water Act. *SSRN Electron. J.* **2015**, 15–41. [[CrossRef](#)]
5. Baran, R.; Kamińska, I.I.; Śrębowata, A.; Dzwigaj, S. Selective hydrodechlorination of 1,2-dichloroethane on NiSiBEA zeolite catalyst: Influence of the preparation procedure on a high dispersion of Ni centers. *Microporous Mesoporous Mater.* **2013**, *169*, 120–127. [[CrossRef](#)]
6. Zichittella, G.; Aellen, N.; Paunović, V.; Amrute, A.P.; Pérez-Ramírez, J. Olefins from Natural Gas by Oxychlorination. *Angew. Chem. Int. Ed.* **2017**, *56*, 13670–13674. [[CrossRef](#)] [[PubMed](#)]
7. Arevalo-Bastante, A.; Álvarez-Montero, M.A.; Bedia, J.; Gómez-Sainero, L.M.; Rodriguez, J.J. Gas-phase hydrodechlorination of mixtures of chloromethanes with activated carbon-supported platinum catalysts. *Appl. Catal. B Environ.* **2015**, *179*, 551–557. [[CrossRef](#)]
8. Chen, J.; Guo, T.; Li, K.; Sun, L. A facile approach to enhancing activity of Ni₂P/SiO₂ catalyst for hydrodechlorination of chlorobenzene: Promoting effect of water and oxygen. *Catal. Sci. Technol.* **2015**, *5*, 2670–2680. [[CrossRef](#)]
9. López, E.; Ordóñez, S.; Sastre, H.; Díez, F.V. Kinetic study of the gas-phase hydrogenation of aromatic and aliphatic organochlorinated compounds using a Pd/Al₂O₃ catalyst. *J. Hazard. Mater.* **2003**, *97*, 281–294. [[CrossRef](#)]
10. Martín-Martínez, M.; Gómez-Sainero, L.M.; Bedia, J.; Arevalo-Bastante, A.; Rodriguez, J.J. Enhanced activity of carbon-supported Pd–Pt catalysts in the hydrodechlorination of dichloromethane. *Appl. Catal. B Environ.* **2016**, *184*, 55–63. [[CrossRef](#)]
11. Bedia, J.; Gómez-sainero, L.M.; Grau, J.M.; Busto, M.; Martín-martínez, M.; Rodriguez, J.J. Hydrodechlorination of dichloromethane with mono- and bimetallic Pd-Pt on sulfated and tungstated zirconia catalysts. *J. Catal.* **2012**, *294*, 207–215. [[CrossRef](#)]
12. de Pedro, Z.M.; Gómez-Sainero, L.M.; González-Serrano, E.; Rodríguez, J.J. Gas-Phase Hydrodechlorination of Dichloromethane at Low Concentrations with Palladium/Carbon Catalysts. *Ind. Eng. Chem. Res.* **2006**, *45*, 7760–7766. [[CrossRef](#)]
13. Chang, W.; Kim, H.; Oh, J.; Ahn, B.J. Hydrodechlorination of chlorophenols over Pd catalysts supported on zeolite Y, MCM-41 and graphene. *Res. Chem. Intermed.* **2018**, *44*, 3835–3847. [[CrossRef](#)]
14. Díaz, E.; Mccall, A.; Faba, L.; Sastre, H.; Ordoñez, S. Trichloroethylene Hydrodechlorination in Water Using Formic Acid as Hydrogen Source: Selection of Catalyst and Operation Conditions. *Environ. Prog. Sustain. Energy* **2012**, *32*, 1217–1222. [[CrossRef](#)]

15. Bonarowska, M.; Kaszukur, Z.; Kepiński, L.; Karpiński, Z. Hydrodechlorination of tetrachloromethane on alumina- and silica-supported platinum catalysts. *Appl. Catal. B Environ.* **2010**, *99*, 248–256. [[CrossRef](#)]
16. Amorim, C.; Wang, X.; Keane, M.A. Application of Hydrodechlorination in Environmental Pollution Control: Comparison of the Performance of Supported and Unsupported Pd and Ni Catalysts. *Chin. J. Catal.* **2011**, *32*, 746–755. [[CrossRef](#)]
17. Lan, L.; Liu, Y.; Liu, S.; Ma, X.; Li, X.; Dong, Z.; Xia, C. Effect of the supports on catalytic activity of Pd catalysts for liquid-phase hydrodechlorination/hydrogenation reaction. *Environ. Technol. (UK)* **2019**, *40*, 1615–1623. [[CrossRef](#)]
18. Álvarez-Montero, M.A.; Gómez-Sainero, L.M.; Juan-Juan, J.; Linares-Solano, A.; Rodriguez, J.J. Gas-phase hydrodechlorination of dichloromethane with activated carbon-supported metallic catalysts. *Chem. Eng. J.* **2010**, *162*, 599–608. [[CrossRef](#)]
19. Bueres, R.F.; Asedegbega-Nieto, E.; Díaz, E.; Ordóñez, S.; Díez, F.V. Performance of carbon nanofibres, high surface area graphites, and activated carbons as supports of Pd-based hydrodechlorination catalysts. *Catal. Today* **2010**, *150*, 16–21. [[CrossRef](#)]
20. Chen, Q.; Wang, M.; Zhang, C.; Ren, K.; Xin, Y.; Zhao, M.; Xing, E. Selectivity Control on Hydrogenation of Substituted Nitroarenes through End-On Adsorption of Reactants in Zeolite-Encapsulated Platinum Nanoparticles. *Chem. Asian J.* **2018**, *13*, 2077–2084. [[CrossRef](#)]
21. Kamińska, I.I.; Lisovytskiy, D.; Casale, S.; Śrębowata, A.; Dzwigaj, S. Influence of preparation procedure on catalytic activity of PdBEA zeolites in aqueous phase hydrodechlorination of 1,1,2-trichloroethene. *Microporous Mesoporous Mater.* **2017**, *237*, 65–73. [[CrossRef](#)]
22. Śrębowata, A.; Tarach, K.; Girman, V.; Góra-Marek, K. Catalytic removal of trichloroethylene from water over palladium loaded microporous and hierarchical zeolites. *Appl. Catal. B Environ.* **2016**, *181*, 550–560. [[CrossRef](#)]
23. Śrębowata, A.; Kamińska, I.I.; Casale, S.; Brouri, D.; Calers, C.; Dzwigaj, S. The impact of the hydrodechlorination process on the physicochemical properties of bimetallic Ag-CuBeta zeolite catalysts. *Microporous Mesoporous Mater.* **2017**, *243*, 56–64. [[CrossRef](#)]
24. Śrębowata, A.; Baran, R.; Łomot, D.; Lisovytskiy, D.; Onfroy, T.; Dzwigaj, S. Remarkable effect of postsynthesis preparation procedures on catalytic properties of Ni-loaded BEA zeolites in hydrodechlorination of 1,2-dichloroethane. *Appl. Catal. B Environ.* **2014**, *147*, 208–220. [[CrossRef](#)]
25. Imre, B.; Hannus, I.; Kiricsi, I. Comparative IR spectroscopic study of Pt- and Pd-containing zeolites in the hydrodechlorination reaction of carbon tetrachloride. *J. Mol. Struct.* **2005**, *744*, 501–506. [[CrossRef](#)]
26. Hannus, I.; Halász, J. Hydrodechlorination over Zeolite Supported Catalysts—Clarification of Reaction Mechanism. *J. Jpn. Pet. Inst.* **2006**, *49*, 105–113. [[CrossRef](#)]
27. Imre, B.; Kónya, Z.; Hannus, I.; Halász, J.; Nagy, J.B.; Kiricsi, I. Hydrodechlorination of chlorinated compounds on different zeolites. In *Studies in Surface Science and Catalysis*; Elsevier: Amsterdam, The Netherlands, 2002; Volume 142A, pp. 927–934.
28. Elola, A.; Díaz, E.; Ordoñez, S. A new procedure for the treatment of organochlorinated off-gases combining adsorption and catalytic hydrodechlorination. *Environ. Sci. Technol.* **2009**, *43*, 1999–2004. [[CrossRef](#)]
29. Fernandez-Ruiz, C.; Bedia, J.; Bonal, P.; Rodriguez, J.J.; Gómez-Sainero, L.M. Chloroform conversion into ethane and propane by catalytic hydrodechlorination with Pd supported on activated carbons from lignin. *Catal. Sci. Technol.* **2018**, *8*, 3926–3935. [[CrossRef](#)]
30. Fernandez-Ruiz, C.; Bedia, J.; Andreoli, S.; Eser, S.; Rodriguez, J.J.; Gómez-Sainero, L.M. Selectivity to Olefins in the Hydrodechlorination of Chloroform with Activated Carbon-Supported Palladium Catalysts. *Ind. Eng. Chem. Res.* **2019**, *58*, 20592–20600. [[CrossRef](#)]
31. Gómez-Sainero, L.M.; Palomar, J.; Omar, S.; Fernández, C.; Bedia, J.; Álvarez-Montero, A.; Rodriguez, J.J. Valorization of chloromethanes by hydrodechlorination with metallic catalysts. *Catal. Today* **2018**, *310*, 75–85. [[CrossRef](#)]
32. Echeandia, S.; Pawelec, B.; Barrio, V.L.; Arias, P.L.; Cambra, J.F.; Loricera, C.V.; Fierro, J.L.G. Enhancement of phenol hydrodeoxygenation over Pd catalysts supported on mixed HY zeolite and Al₂O₃. An approach to O-removal from bio-oils. *Fuel* **2014**, *117*, 1061–1073. [[CrossRef](#)]
33. Sato, K.; Nishimura, Y.; Matsubayashi, N.; Imamura, M.; Shimada, H. Structural changes of Y zeolites during ion exchange treatment: Effects of Si/Al ratio of the starting NaY. *Microporous Mesoporous Mater.* **2003**, *59*, 133–146. [[CrossRef](#)]

34. Ma, Z.; Hu, H.; Sun, Z.; Fang, W.; Zhang, J.; Yang, L.; Zhang, Y.; Wang, L. Acidic Zeolite L as a Highly Efficient Catalyst for Dehydration of Fructose to 5-Hydroxymethylfurfural in Ionic Liquid. *ChemSusChem* **2017**, *10*, 1669–1674. [[CrossRef](#)]
35. de Oliveira, A.M.; Baibich, I.M.; Machado, N.R.C.F.; Mignoni, M.L.; Pergher, S.B.C. Decomposition of nitric oxide on Pd-mordenite. *Catal. Today* **2008**, *133–135*, 560–564. [[CrossRef](#)]
36. Sato, K.; Nishimura, Y.; Honna, K.; Matsubayashi, N.; Shimada, H. Role of HY zeolite mesopores in hydrocracking of heavy oils. *J. Catal.* **2001**, *200*, 288–297. [[CrossRef](#)]
37. Sato, K.; Nishimura, Y.; Shimada, H. Preparation and activity evaluation of Y zeolites with or without mesoporosity. *Catal. Lett.* **1999**, *60*, 83–87. [[CrossRef](#)]
38. Cano, M.; Guarín, F.; Aristizábal, B.; Villa, A.-L.; González, L.-M. Catalytic activity and stability of Pd/Co catalysts in simultaneous selective catalytic reduction of NO_x with methane and oxidation of o-dichlorobenzene. *Catal. Today* **2017**, *296*, 105–117. [[CrossRef](#)]
39. Lambrou, P.S.; Polychronopoulou, K.; Petalidou, K.C.; Efstathiou, A.M. Oxy-chlorination as an effective treatment of aged Pd/CeO₂-Al₂O₃ catalysts for Pd redispersion. *Appl. Catal. B Environ.* **2012**, *111*, 349–359. [[CrossRef](#)]
40. Chandra Shekar, S.; Krishna Murthy, J.; Kanta Rao, P.; Rama Rao, K.S. Selective hydrogenolysis of dichlorodifluoromethane on carboncovered alumina supported palladium catalyst. *Catal. Commun.* **2003**, *4*, 39–44. [[CrossRef](#)]
41. Bhogeswararao, S.; Srinivas, D. Catalytic conversion of furfural to industrial chemicals over supported Pt and Pd catalysts. *J. Catal.* **2015**, *327*, 65–77. [[CrossRef](#)]
42. Feeley, J.S.; Sachtler, W.M.H. Palladium-enhanced reducibility of nickel in NaY. *Zeolites* **1990**, *10*, 738–745. [[CrossRef](#)]
43. Seshu Babu, N.; Lingaiah, N.; Sai Prasad, P.S. Characterization and reactivity of Al₂O₃ supported Pd-Ni bimetallic catalysts for hydrodechlorination of chlorobenzene. *Appl. Catal. B Environ.* **2012**, *111*, 309–316. [[CrossRef](#)]
44. McCusker, L.B.; Olson, D.H.; Baerlocher, C. *Atlas of Zeolite Framework Types*; Elsevier: Amsterdam, The Netherlands, 2007; ISBN 9780444530646.
45. Velaga, B.; Parde, R.P.; Soni, J.; Peela, N.R. Synthesized hierarchical mordenite zeolites for the biomass conversion to levulinic acid and the mechanistic insights into humins formation. *Microporous Mesoporous Mater.* **2019**, *287*, 18–28. [[CrossRef](#)]
46. Tangale, N.P.; Niphadkar, P.S.; Joshi, P.N.; Dhepe, P.L. Hierarchical K/LTL zeolite as solid base for aqueous phase hydrogenation of xylose to xylitol. *Microporous Mesoporous Mater.* **2019**, *278*, 70–80. [[CrossRef](#)]
47. Treacy, M.M.J. *Collection of Simulated XRD Powder Patterns for Zeolites*; Elsevier Science: Amsterdam, The Netherlands, 2001.
48. Pearce, H.A. Zeolite molecular sieves—Structure, chemistry and use. *J. Chromatogr. A* **1975**, *106*, 499. [[CrossRef](#)]
49. Dantas Ramos, A.L.; da Silva Alves, P.; Aranda, D.A.G.; Schmal, M. Characterization of carbon supported palladium catalysts: Inference of electronic and particle size effects using reaction probes. *Appl. Catal. A Gen.* **2004**, *277*, 71–81. [[CrossRef](#)]
50. Briggs, D.; Wanger, C.D.; Riggs, W.M.; Davis, L.E.; Moulder, J.F.; E. Muilenberg, G. *Handbook of X-ray Photoelectron Spectroscopy*; Chastain, J., Ed.; Perkin-Elmer Corporation, Physical Electronics Division: Eden Prairie, MN, USA, 1981.
51. Gamero, M.; Aguayo, A.T.; Ateka, A.; Pérez-Uriarte, P.; Gayubo, A.G.; Bilbao, J. Role of Shape Selectivity and Catalyst Acidity in the Transformation of Chloromethane into Light Olefins. *Ind. Eng. Chem. Res.* **2015**, *54*, 7822–7832. [[CrossRef](#)]
52. Bonarowska, M.; Kaszkur, Z.; Łomot, D.; Rawski, M.; Karpiński, Z. Effect of gold on catalytic behavior of palladium catalysts in hydrodechlorination of tetrachloromethane. *Appl. Catal. B Environ.* **2015**, *162*, 45–56. [[CrossRef](#)]
53. Sánchez, C.A.G.; Patiño, C.O.M.; de Correa, C.M. Catalytic hydrodechlorination of dichloromethane in the presence of traces of chloroform and tetrachloroethylene. *Catal. Today* **2008**, *133*, 520–525. [[CrossRef](#)]

54. Bedia, J.; Arevalo-Bastante, A.; Grau, J.M.; Dosso, L.A.; Rodriguez, J.J.; Mayoral, A.; Diaz, I.; Gómez-Sainero, L.M. Effect of the Pt-Pd molar ratio in bimetallic catalysts supported on sulfated zirconia on the gas-phase hydrodechlorination of chloromethanes. *J. Catal.* **2017**, *352*, 562–571. [[CrossRef](#)]
55. Martín-Martínez, M.; Gómez-Sainero, L.M.; Álvarez-Montero, M.A.; Bedia, J.; Rodríguez, J.J. Comparison of different precious metals in activated carbon-supported catalysts for the gas-phase hydrodechlorination of chloromethanes. *Appl. Catal. B Environ.* **2013**, *132*, 256–265. [[CrossRef](#)]



© 2020 by the authors. Licensee MDPI, Basel, Switzerland. This article is an open access article distributed under the terms and conditions of the Creative Commons Attribution (CC BY) license (<http://creativecommons.org/licenses/by/4.0/>).